

THE UNIVERSITY OF NEW MEXICO  
HEALTH SCIENCES CENTER  
COLLEGE OF PHARMACY  
ALBUQUERQUE, NEW MEXICO

The University of New Mexico

Correspondence Continuing Education Courses  
for  
Nuclear Pharmacists and Nuclear Medicine Professionals

VOLUME VII, NUMBER 5

PART I

*Pharmacokinetics and Positron Emission Tomography*

by:

Laura L. Boles Ponto, PhD  
James A. Ponto, MS

The University of New Mexico Health Sciences Center College of Pharmacy is approved by the American Council on Pharmaceutical Education as a provider of continuing pharmaceutical education. Program No. 039-000-98-001-H04. 2.5 Contact Hours or .25 CEU's



# Pharmacokinetics and Positron Emission Tomography

by:

Laura L. Boles Ponto, PhD  
James A. Ponto, MS

## *Coordinating Editor*

and

## *Director of Pharmacy Continuing Education*

William B. Hladik III, MS, RPh  
College of Pharmacy  
University of New Mexico Health Sciences Center

## *Managing Editor*

Julliana Newman, ELS  
Wellman Publishing, Inc.

## *Associate Editor and Production Specialist*

Sharon I. Magers Ramirez, Administrative Assistant II  
College of Pharmacy  
University of New Mexico Health Sciences Center

## *Editorial Board*

George H. Hinkle, MS, RPh, BCNP  
William B. Hladik III, MS, RPh  
Jeffrey P. Norenberg, MS, RPh, BCNP  
Laura L. Boles Ponto, PhD, RPh  
Timothy M. Quinton, PharmD, MS, RPh, BCNP

## **Guest Reviewer**

Ken Breslow, MS, RPh  
Stephen M. Moerlein, PhD

While the advice and information in this publication are believed to be true and accurate at press time, neither the author(s) nor the editor nor the publisher can accept any legal responsibility for any errors or omissions that may be made. The publisher makes no warranty, express or implied, with respect to the material contained herein.

Copyright 1998  
University of New Mexico Health Sciences Center  
Pharmacy Continuing Education  
Albuquerque, New Mexico

# PHARMACOKINETICS AND POSITRON EMISSION TOMOGRAPHY

by:

Laura L. Boles Ponto, Ph.D.  
James A. Ponto, M.S.

University of Iowa  
Department of Radiology  
PET Imaging Center  
Iowa City, Iowa 52242

## STATEMENT OF OBJECTIVES

The purpose of this lesson is to provide information involving the unique, mutually-beneficial relationship between PET imaging and pharmacokinetics. Specifically, the applications of pharmacokinetics in PET imaging in order to derive quantitative measures of physiological function and the use of PET imaging as a tool to study the pharmacokinetics of specific drugs will be discussed.

*This lesson is designed as both an introduction to the interplay of PET imaging and pharmacokinetics as well as a resource for PET applications (e.g., receptor agents, clinical and research uses of FDG). The reader is not expected to be able to apply the models and imaging techniques described in this lesson, but rather to know that these models and techniques exist and to have available the necessary references to apply them if needed.*

**Upon successful completion of this lesson, the reader should be able to:**

1. Discuss the applicability and use of pharmacokinetics (tracer kinetic models) in PET imaging to measure physiologic processes.
2. List common types of compartmental and non-compartmental models used for PET radiopharmaceuticals and cite at least one example for each.
3. Discuss the applicability and use of PET imaging as a pharmacokinetic tool to assess radiolabeled drug disposition.
4. List pharmacokinetic issues that can be addressed *in vivo* by PET imaging and cite at least one example for each.
5. Describe practical limitations of PET imaging in performing clinical investigations involving pharmacokinetics.

## **COURSE OUTLINE**

### **I. INTRODUCTION**

### **II. CAPABILITIES AND LIMITATIONS OF PET**

### **III. THE USE OF PHARMACOKINETICS IN PET**

- A. One-compartment Model: [<sup>15</sup>O]Water
- B. Two-Compartment Model: [<sup>11</sup>C]Acetate
- C. Three-Compartment Model: [<sup>18</sup>F]Fluorodeoxyglucose
- D. Three or Four Compartment, Capacity-limited Model:  
[<sup>11</sup>C]Raclopride and N-[<sup>11</sup>C]methylspiperone
- E. Non-compartmental Analysis
  - 1. Mean Transit Time
  - 2. Standardized Uptake Values (SUV)
  - 3. Multiple-Time/Graphical Approach (The Patlak Method)

### **IV. THE USE OF PET IN PHARMACOKINETICS**

- A. "Imageable Biodistribution": General Considerations
- B. CNS Pharmacokinetics/dynamics
- C. Route of Administration: I.A. versus I.V.
- D. Receptor Binding and Occupancy
  - 1. Dopamine-D<sub>2</sub> Receptors
  - 2. Mu-Opiate Receptors
- E. Toxicodynamics: Alcohol
- F. Influence of Enantiomeric Forms
  - 1. Nicotine
  - 2. Cocaine

### **V. CONCLUSION**

## Introduction

Positron emission tomography (PET), unlike its tomographic counterparts computed tomography (CT) or magnetic resonance imaging (MRI), produces functional, as opposed to anatomical, images. Clinically, these functional images represent a mapping of physiological and/or pharmacological processes *in vivo*, e.g., blood flow to the heart, glucose metabolism in the brain, binding of a pharmaceutical (ligand) to its specific receptor or binding site. Technically, these functional images are the culmination of the combination of the unique characteristics of the positron-emitting radiopharmaceuticals, the technological developments which make positron emission coincidence detection feasible, the refinement of reconstruction algorithms, and the development and application of workable tracer kinetic models.

It will be the purpose of this paper to discuss the unique relationship between PET imaging and pharmacokinetics. This relationship is one of mutual benefit. The strength of PET as an imaging modality is that it produces temporally and spatially identifiable quantitative images expressed in physiologically meaningful units (e.g., blood flow expressed as mL/min/100 gm tissue). This is the result of the application of pharmacokinetics. On the other hand, PET is a pharmacokinetic tool which allows one to visualize and quantify processes, *in vivo*, which were in the past little more than mathematical constructs.

This lesson is designed as both an introduction to the interplay of PET imaging and pharmacokinetics as well as a resource for PET applications (e.g., receptor agents, clinical and research uses of FDG). The reader is not expected to

be able to apply the models and imaging techniques described in this lesson, but rather to know that these models and techniques exist and to have available the necessary references to apply them if needed. The major emphasis of this pharmacokinetic discussion will be on the assumptions and limitations inherent in the formulation and application of tracer kinetic models. Although the discussion is centered on PET radiopharmaceuticals, as SPECT analogs (e.g., [ $^{123}\text{I}$ ]iodobenzofuran for dopamine- $\text{D}_2$  receptors<sup>1</sup> are developed, these same concepts will be applicable. In addition, kinetic analysis in conventional nuclear medicine is becoming more important. Whether it is a standardized uptake value for an oncologic imaging agent or a mean residence time used for the calculation of individual radiation dosimetry for a therapeutic radiopharmaceutical, the same principles as detailed for PET will apply. The nuclear pharmacist, as the only nuclear medicine team member with both pharmacological and pharmacokinetic training, needs to understand the concepts and applications of tracer kinetic modeling. To facilitate the varying needs of readers, part of the more detailed mathematical explanations and resource materials have been moved to appendices and operational equations (i.e., the equations actually used in final calculations) are highlighted by a boxed border.

### **Capabilities and Limitations of PET**

A positron is a positively-charged electron (i.e., antimatter). Positron-emitting nuclides are produced by bombarding target material with protons or deuterons in a cyclotron. The resulting nuclide is unstable (i.e., the nucleus is

neutron-deficient), and therefore, stabilizes through decay by positron-emission. The emitted positron travels a finite distance (statistically defined by the energy at which it is emitted from the nucleus) before coming into contact with a negatively-charged electron (i.e., matter). The positron-electron (matter-antimatter) interaction results in the annihilation of the two particles and the release of radiation. This conversion is in the form of two 511 keV gamma ( $\gamma$ ) rays emitted at 180° angle from each other. These coincident  $\gamma$  rays are then detected by the PET camera or scanner which consists of a ring of detectors positioned around the patient.

The advantages and disadvantages of this modality lie primarily with the positron-emitting nuclides. The primary advantages are two-fold:

1. The decay process produces the two 511 keV  $\gamma$  rays which are of an energy and geometric orientation for optimal detection and image reconstruction.
2. The major positron-emitting species,  $^{15}\text{O}$ -oxygen,  $^{13}\text{N}$ -nitrogen,  $^{11}\text{C}$ -carbon, and  $^{18}\text{F}$ -fluorine, unlike those utilized in conventional nuclear medicine, are isotopes of elements which are components of essentially all molecules of biological interest, i.e., naturally-occurring biological molecules, biologically-relevant ionic species, analogs of biological molecules or ions, or drugs.

The primary disadvantages stem from the short physical half-lives of these positron-emitting nuclides (See Table 1 ). These half-lives (i.e., 2 to 110 minutes for the commonly used nuclides listed in Table 1) require that nuclide production, chemical synthesis, and pharmaceutical quality control testing all be performed on-

**Table 1. Positron-Emitting Radionuclides Used in PET Radiopharmaceuticals**

<b>Nuclide</b>	<b>t<sub>1/2</sub> (minutes)</b>	<b>Reaction to Produce</b>	<b>Production Method</b>
<sup>15</sup> O	2.07	<sup>14</sup> N(d,n) <sup>15</sup> O <sup>15</sup> N(p,n) <sup>15</sup> O	Cyclotron
<sup>13</sup> N	9.96	<sup>16</sup> O(p,α) <sup>13</sup> N <sup>13</sup> C(p,n) <sup>13</sup> N	Cyclotron
<sup>11</sup> C	20.4	<sup>14</sup> N(p,α) <sup>11</sup> C	Cyclotron
<sup>18</sup> F	109.7	<sup>18</sup> O(p,n) <sup>18</sup> F	Cyclotron
<sup>82</sup> Rb	1.25	Decay of <sup>82</sup> Sr	Generator

site. This is a facilities— and labor—intensive proposition<sup>2-10</sup>. A PET production and imaging center requires both a cyclotron and a dedicated PET scanner. Far less expensive, but much more limited in capability, are PET centers that utilize only radiopharmaceuticals that are generator-produced (e.g., <sup>82</sup>Rb-rubidium chloride) or commercially available (e.g., fluorinated radiopharmaceuticals from centralized production facilities in some geographic areas) and lower-priced imaging alternatives such as high-energy collimated SPECT cameras or coincidence cameras<sup>11</sup>.

An additional disadvantage is that the short half-lives mandate that synthetic and quality control (Q.C.) components of radiopharmaceutical production be limited to 3 half-lives or less. For example, in the case of <sup>11</sup>C-containing compounds, synthesis and Q.C. of formulated product must be accomplished in 1 hour or less. Because of these time constraints, only fluorinated radiopharmaceuticals are potential candidates for centralized production and commercial availability.

Currently, USP monographs, which serve as recognized drug standards, are available for a number of PET radiopharmaceuticals (See Table 2.). Under the provisions of the Food and Drug Administration Modernization Act of 1997, producers and/or manufacturers of PET radiopharmaceuticals are not required to register as a drug establishment or to file an NDA or ANDA for a period not to be less than 4 years from enactment (i.e., November 21, 2001)<sup>12</sup>. However, all PET radiopharmaceuticals must meet USP standards for the specific agent, when available, as well as the provisions in the USP chapter entitled “Radiopharmaceuticals for Positron Emission Tomography - Compounding”<sup>13</sup>.

**Table 2. Radiopharmaceuticals for Positron Imaging: USP Monographs (modified from Larson, 1998<sup>12</sup>)**

Fludeoxyglucose F 18 (also known as [ <sup>18</sup> F]fluoro-2-deoxyglucose, FDG)
Fluorodopa F 18
Water O 15
Sodium acetate C 11
Carbon monoxide C 11
Sodium fluoride F 18
Methionine C 11
Mespiperone C 11 (also known as N-[ <sup>11</sup> C]methylspiperone)
Raclopride C 11
Rubidium chloride Rb 82
Ammonia N 13
Flumazenil C 11 (pending)

## The Use of Pharmacokinetics in P.E.T

The raw images produced by the PET camera are three-dimensional reconstructions of count-rate distributions. These images are qualitative or semi-quantitative in nature and are frequently of only limited value to the clinician/scientist. The transformation into quantitative, functionally-based images requires the application of tracer kinetic models<sup>14-15</sup>. These models mathematically relate observable components of the system (e.g., count rate distributions in various anatomical spaces, arterial input functions) to functional processes. The model development process is one by which a comprehensive model (i.e., one incorporating all known, relevant information about the behavior of the tracer in the body or organ of interest) is reduced to a workable form<sup>14</sup>. Model reduction is accomplished through the formulation and application of simplifying assumptions. For the most part, compartmental approaches have been utilized in the formulation of tracer kinetic models in P.E.T\*. See Table 3 for representative examples.

### One-compartment Model: [<sup>15</sup>O]Water

---

\* Unlike the majority of authors reporting in the pharmacokinetic literature who use the double subscript notation (i.e., "to-from" scheme) for the designation of rate constants, the PET literature utilizes the sequential numbering system. All models will be reported in this paper utilizing the notation adopted by the developers and users of the particular model. No attempt will be made to standardize the notation throughout this work.

**Table 3. Examples of Applications of Pharmacokinetic/dynamic Approaches to PET Tracer Kinetic Modeling**

Type of Model	Pharmaceutical	Function	Organ(-s)	Basis
One-compartment	[ <sup>15</sup> O]water	Blood flow	heart, brain, skeletal muscle, liver, tumor	Theoretical
Two-compartment	[ <sup>11</sup> C]acetate	Oxygen consumption	heart	Empirical
Three-compartment	[ <sup>18</sup> F]fluoro-2-deoxyglucose	Glucose metabolism	heart, brain, tumor	Theoretical
Three-compartment/ capacity limited	[ <sup>11</sup> C]raclopride [ <sup>11</sup> C]flumazenil	Receptor binding	brain	Theoretical
Four-compartment	N-[ <sup>11</sup> C]methyispiperone	Receptor binding	brain	Theoretical
Non-compartmental	1-[ <sup>11</sup> C]methionine	Amino acid metabolism	brain, tumor	Theoretical

[<sup>15</sup>O]Water is a tracer utilized to determine regional blood flow. The theory behind this application is based on Kety-Schmidt's single compartment model for diffusible tracers<sup>16-20</sup>. Water exists in the body in three potential compartments — the vascular space, the interstitial space, and the cellular space. Because the transport of water, whether naturally-occurring [<sup>16</sup>O]water or radioactive [<sup>15</sup>O]water, across the capillary wall is very fast, especially in respect to blood flow (i.e., delivery of tracer), all three spaces can be considered as a single compartment. Under these conditions, the concentration of [<sup>15</sup>O]water in the tissue of interest is a function of the blood flow to, and the volume of distribution (or partition coefficient) of, that tissue. Blood flow delivers tracer to the tissue as well as clears tracer from the tissue. The amount of radioactivity is also reduced by radioactive decay.

Two approaches (i.e., dynamic and static imaging) have been utilized to determine blood flow from [<sup>15</sup>O]water data, with the choice of approach dependent on the type of PET data acquired.

In the case where dynamic data (i.e., multiple scans) are acquired over an extended period of time (i.e., 6 to 10 minutes), the following equations have been utilized<sup>14, 21-23</sup>:

$$F = \frac{\int Q^* dt [\lambda \int Q dt + Q(T)] - Q^*(T) \int Q dt}{\int C_i dt \int Q^* dt - \int Q dt \int C_i^* dt}$$

$$V = \frac{\int Q^* dt [\lambda \int Q dt + Q(T)] - Q^*(T) \int Q dt}{\int C_i^* dt [\lambda \int Q dt + Q(T)] - Q^*(T) \int C_i dt}$$

$$Q(t) = C(t) V$$

where  $F$  = blood flow (mL/min/g);  $V$  = distribution volume (mL/g) of the tracer;  $Q(t)$  = total radioactivity ( $\mu\text{Ci}$ ) in the element at time =  $t$ ;  $C_i(t)$  = tracer concentration ( $\mu\text{Ci/mL}$ ) in arterial blood at time =  $t$ ;  $C(t)$  = tracer concentration ( $\mu\text{Ci/mL}$ ) in the element at time =  $t$ ; and  $\lambda$  = physical decay constant of the radioactive tracer. All terms denoted by an asterisk are decayed-corrected quantities.

Implementation of this approach requires: 1) measurements of total [ $^{15}\text{O}$ ] activity in regions of interest from time = 0 to  $T$ ; 2) measurements of total [ $^{15}\text{O}$ ] activity in arterial blood from time = 0 to  $T$ ; and 3) assumption that  $Q(0) = 0$ . If  $T$  is chosen such that  $Q(T) \approx 0$ , then the equations become:

$$F = \frac{\lambda \int Q^* dt \int Q dt - Q^*(T) \int Q dt}{\int C_i dt \int Q^* dt - \int Q dt \int C_i^* dt}$$

$$V = \frac{\lambda \int Q^* dt - Q^*(T)}{\lambda \int C_i^* dt - \frac{Q^*(T) \int C_i dt}{\int Q dt}}$$

When a single static image is acquired, the following equation for the relationship between the activity in the tissue is utilized<sup>24-27</sup>:

$$C_t(t) = f C_a(t) \otimes e^{-[(f/p)+\lambda]t}$$

where  $C_t(t)$  = time varying radioactivity concentration ( $\mu\text{Ci/mL}$ ) in tissue;  $C_a(t)$  = time varying radioactivity concentration ( $\mu\text{Ci/mL}$ ) in arterial blood;  $f$  = local mass

specific blood flow (mL of blood/mL of brain/min);  $p$  = tissue-blood partition coefficient for water (mL of blood/mL of brain);  $\lambda$  = decay constant for [ $^{15}\text{O}$ ]; and  $\otimes$  = mathematical operation of convolution. It should be emphasized that PET images are not instantaneous count rates, but rather are the counts determined over a finite period of time. Therefore, the determined count rate values are represented by the integral over the scanning interval ( $t = T_1$  to  $T_2$ ). By assuming a fixed value of tissue-blood partition coefficient,  $p$  (such as 0.9 mL of blood/mL of brain<sup>27</sup>), the equation:

$$\int_{T_1}^{T_2} C_t(t) dt = f \int_{T_1}^{T_2} C_a(t) \otimes e^{-[(f/p)+\lambda]t} dt$$

has only one unknown,  $f$ , which can be estimated by using a look-up table or an analytic relationship<sup>27</sup>. Implementation of this approach requires: 1) measurement of total [ $^{15}\text{O}$ ] activity in regions of interest from time =  $T_1$  to  $T_2$ ; and 2) measurements of total [ $^{15}\text{O}$ ] activity in arterial blood from time = 0 to  $T$ . By excluding the first 40 seconds of data, errors associated with the blood-borne radioactivity component in measured PET data and the differences in arrival time of an arterial bolus across the various brain regions are minimized.

The latter described approach, known as the autoradiographic method, is currently the most frequently applied quantitative methodology employed for "brain mapping" work. In a review of the brain mapping literature from 1995 to 1998, 80% of the studies specified the use of I.V. bolus administration and 45% of the studies utilized the autoradiographic method of quantitative analysis.

Implementation of this method is technically challenging but has been completely

detailed by Hichwa, et al.<sup>28</sup>. In addition, this methodology has been extended to examine blood flow in skeletal muscle<sup>29-30</sup>, liver<sup>31</sup> and solid tumors<sup>32</sup>.

### Two-Compartment Model: [<sup>11</sup>C]Acetate

[<sup>11</sup>C]Acetate can be applied as a tracer of myocardial tricarboxylic acid (TCA) cycle flux<sup>33-34</sup> and therefore, an *in vivo* measure of myocardial oxidative metabolism. The disposition of [<sup>11</sup>C]acetate in the myocardium after intravenous administration has been modeled, empirically, with a monoexponential or a biexponential function during rest and exercise, respectively:

$$Q = A_1 e^{-k_1 t}$$
$$Q = A_1 e^{-k_1 t} + A_2 e^{-k_2 t}$$

where Q = myocardial [<sup>11</sup>C] activity, A<sub>1</sub> and A<sub>2</sub> = constants, k<sub>1</sub> and k<sub>2</sub> = myocardial turnover rate constants for the initial and terminal phases, respectively, and t = time post-peak activity<sup>35-36</sup>. The initial rapidly clearing phase of the biexponential relationship constitutes > 80% of the area under the curve<sup>37</sup>. Various theoretical models have been proposed to explain the observed time-activity relationship<sup>38-42</sup>. Because of the difficulty in fitting the second exponential with data available from PET studies, some researchers have fit only the initial linear portion of the myocardial time-activity curves to derive the turnover rate constant, k<sub>mono</sub><sup>36,43</sup>. The values for k<sub>mono</sub> exhibit relatively high correlations with k<sub>1</sub> values (i.e., r = 0.95)<sup>44</sup>. The clearance rate constant, k, has also been determined using the mean transit time<sup>45</sup> (See Non-compartmental Analysis: Mean Transit Time.). Image analysis algorithms have been developed to produce parametric images (i.e., images in which the value assigned to a particular pixel is that of a derived

parameter value (e.g.,  $k_1$ ) as opposed to an observed quantity (i.e., count rate)<sup>45-46</sup>).

Myocardial oxygen consumption ( $MVO_2$ ), calculated from the product of flow and the measured oxygen extraction in aortic and coronary sinus catheterized dogs<sup>47</sup>, has been related to the  $k_1$  value by linear regression<sup>33,36</sup>. These relationships determined in dogs have been applied to the calculation of myocardial oxygen consumption in healthy and diseased humans<sup>35-36</sup>. Both the  $k_1$  and  $k_{mono}$  parameter values have also been related to indirect measures of  $MVO_2$  such as rate pressure product (RPP)<sup>43,48</sup>. Recent work<sup>49</sup> has related direct measurements of  $MVO_2$  in humans to calculated  $k_1$  and  $k_{mono}$  parameter values via linear regression:

$$k_1 \text{ (min}^{-1}\text{)} = 0.0139 + 0.0041 \times MVO_2 \text{ (mL/min/100g)}$$

$$k_{mono} \text{ (min}^{-1}\text{)} = 0.0197 + 0.0027 \times MVO_2 \text{ (mL/min/100g)}$$

Modifications to the model and data acquisition and analysis scheme have been developed that allow for the calculation of both myocardial oxygen consumption and myocardial blood flow with a single administration of only [<sup>11</sup>C]acetate<sup>42,49</sup>.

### **Three-Compartment Model: [<sup>18</sup>F]Fluorodeoxyglucose**

[<sup>18</sup>F]Fluorodeoxyglucose (FDG), the most widely studied of all PET tracers, is a glucose analog utilized as a metabolic tracer, and therefore, is used to measure tissue viability. This agent has been utilized traditionally as a marker of metabolic activity in the brain<sup>50</sup> and in the heart<sup>51</sup>, but more recently, the use of FDG for oncology has literally exploded<sup>52</sup>. A comprehensive review of the uses of

FDG is beyond the scope of this lesson. However Appendix 1 presents an overview of FDG uses with relevant citations.

The three compartment model utilized to analyze FDG biodistribution data is an extension of the model originally developed for [ $^{14}\text{C}$ ]deoxyglucose by Sokoloff<sup>53</sup>. See Figure 1 for schematic<sup>53-54</sup>. In this model, the FDG exists in the plasma as FDG and in the tissue as either FDG or as FDG-6-P (fluorodeoxyglucose-6-phosphate) with the concentrations of the compartments designated as  $C_p^*$ ,  $C_e^*$  or  $C_m^*$ , respectively. The parameters,  $k_1^*$  and  $k_2^*$ , represent the passive and/or active transport from the plasma into and out of the tissue of interest (which for the brain is transport across the blood-brain barrier) and the parameters,  $k_3^*$  and  $k_4^*$ , represent the phosphorylation and de-phosphorylation of FDG, respectively.

The use of this workable model for the calculation of glucose metabolic rates is predicated on the following assumptions<sup>53-55</sup>:

1. FDG kinetic behavior patterns the kinetic behavior of glucose (G) in that they compete for common transport carriers and hexokinase-mediated phosphorylation and that the differences in disposition can be accounted for by a lumped constant, LC.
2. A compartmental model is appropriate because the transport and phosphorylation obeys first-order kinetics and are homogeneous within a local region (i.e., ROI or pixel).
3. FDG-6-P is not subject to further metabolism, except for the dephosphorylation reaction, and therefore, is trapped within the tissue.

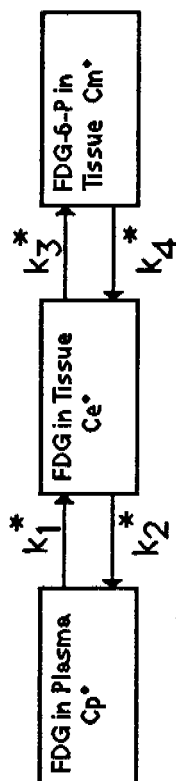


**Figure 1.** Three compartment model derived for FDG.  $C_p^*$  is the concentration of FDG in the plasma,  $C_e^*$  is the concentration of FDG in the tissue,  $C_m^*$  is the concentration of FDG-6-P in the tissue, and  $k_1^*$  -  $k_4^*$  are the first order rate constants describing transfer between compartments.

4. The metabolism of G is at steady-state throughout the time-course of study such that the plasma glucose concentration remains constant and unaffected by the FDG concentration.
5. For both FDG and G, the arterial plasma concentrations and capillary plasma concentrations are approximately equal.

The concentrations in the two tissue compartments can be described by the following equations<sup>14,54,56</sup>:

$$C_e^* = \frac{k_1^* k_3^*}{\alpha_2 - \alpha_1} [(k_4^* - \alpha_1) e^{-\alpha_1 t} + (\alpha_2 - k_4^*) e^{-\alpha_2 t}] \otimes C_p^*(t)$$

$$C_m^* = \frac{k_1^*}{\alpha_2 - \alpha_1} [e^{-\alpha_1 t} + e^{-\alpha_2 t}] \otimes C_p^*(t)$$

where  $C_p^*$  = concentration of FDG in plasma,  $C_e^*$  = concentration of FDG in tissue,  $C_m^*$  = concentration of FDG-6-P in tissue,  $k_1^*$  through  $k_4^*$  are the first order rate constants, and

$$\alpha_1, \alpha_2 = \frac{(k_2^* + k_3^* + k_4^*) \mp \sqrt{(k_2^* + k_3^* + k_4^*)^2 - 4k_2^*k_4^*}}{2}$$

Since PET imaging can not distinguish between the chemical forms of FDG nor vascular and non-vascular activity, the equation for the  $^{18}\text{F}$  activity in the tissue  $C_i^*$  is:

$$C_i^* = \frac{k_1^*}{\alpha_2 - \alpha_1} [(k_3^* + k_4^* - \alpha_1) e^{-\alpha_1 t} + (\alpha_2 - k_3^* - k_4^*) e^{-\alpha_2 t}] \otimes C_p^*(t) + V_b C_p^*(t)$$

where  $V_b$  is the vascular volume in the tissue of interest. The FDG concentration in whole blood is assumed to be equal to that in plasma in this application.

The use of the above equations requires dynamic PET acquisition, i.e., multiple samples of tissue tracer activity ( $C_i^*(t)$  as a function of time) and continuous plasma sampling ( $C_p^*(t)$  as a function of time) over the time course of the study. The kinetic data are then fitted to the three compartment model for parameter estimation. The estimated parameter values are then utilized to estimate the metabolic rate of glucose (MRGlc) for the tissue or region of interest:

$$\text{MRGlc} = \frac{C_p}{LC} \frac{k_1^* k_3^*}{k_2^* + k_3^*}$$

where  $C_p$  = plasma glucose concentration and LC = lumped constant.

The metabolic rate of glucose ( $R_i$ ) can also be determined after a single static image acquisition after an appropriate time, T. This method requires, in addition to the [ $^{18}\text{F}$ ] activity at time T ( $C_i^*$ ), a complete history of the FDG concentration in the blood from time = 0 to T ( $C_p^*(t)$ ) and a single plasma concentration of glucose,  $C_p$ .

The operational equation becomes<sup>54</sup>:

$$R_i = \frac{C_p \left( C_i^*(T) - \frac{k_1^*}{\alpha_2 - \alpha_1} [ (k_4^* - \alpha_1)e^{-\alpha_1 t} + (\alpha_2 - k_4^*)e^{-\alpha_2 t} ] \otimes C_p^*(t) \right)}{LC \frac{k_2^* + k_3^*}{\alpha_2 - \alpha_1} (e^{-\alpha_1 t} - e^{-\alpha_2 t}) \otimes C_p^*(t)}$$

where all parameters are as defined above. A number of modifications to this relationship have been proposed, including the use of population averages for various parameter values<sup>57-58</sup>, fixing certain parameter values<sup>59</sup> (e.g.,  $k_4$ ), and Bayes estimation techniques<sup>60</sup>. The sources of error and limitations of the above described quantitative methods as applied to FDG have been reviewed by Alavi<sup>61</sup> and by Schmidt<sup>62</sup>.

### Three or Four Compartment, Capacity-limited Model:

#### [<sup>11</sup>C]Raclopride and N-[<sup>11</sup>C]methylospiperone

Radiolabeled ligands have been utilized to map and quantify various types of receptors in the brain, heart, and other organs, both *in vitro* and more recently with PET *in vivo*<sup>63</sup>. Although a number of different receptor systems have been explored with PET (See Appendix 2.), the most widely studied, especially that related to the formulation of receptor-binding models, has been directed to the dopamine-D<sub>2</sub> system. This receptor system has been investigated primarily with [<sup>11</sup>C] or [<sup>18</sup>F]- labeled spiperone (spiroperidol) and its derivatives (N-methyl or fluoroethylspiperone)<sup>64-73</sup> or with the benzamide compound, [<sup>11</sup>C]raclopride<sup>74-80</sup>.

Six components form the conceptual framework for the comprehensive model of receptor-binding<sup>14</sup>. The six components are:

1. Delivery of ligand to the tissue of interest via blood flow.
2. Free ligand in plasma.
3. Free ligand in tissue.
4. Non-specifically bound ligand in tissue.
5. Free ligand in synapses or in biophase adjacent to receptor.
6. Specifically bound ligand in synapses or in biophase adjacent to receptor.

In PET applications, the comprehensive model is generally reduced to a three or four compartment model<sup>14,46,67,69,71,79,81-85</sup>. See Figure 2. In these models, C<sub>p</sub> is the concentration of tracer (i.e., labeled ligand) in plasma, C<sub>f</sub> is the free tracer in tissue, C<sub>ns</sub> is the non-specifically bound tracer in tissue, and C<sub>b</sub> is the specifically bound tracer in tissue. These reduced models are based on three assumptions:

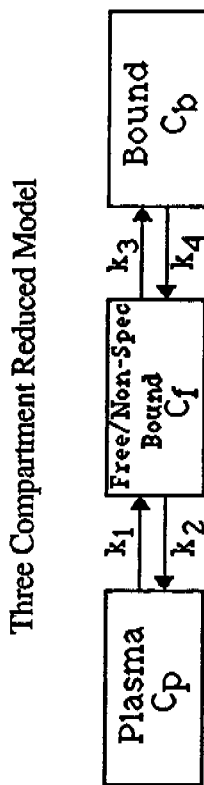
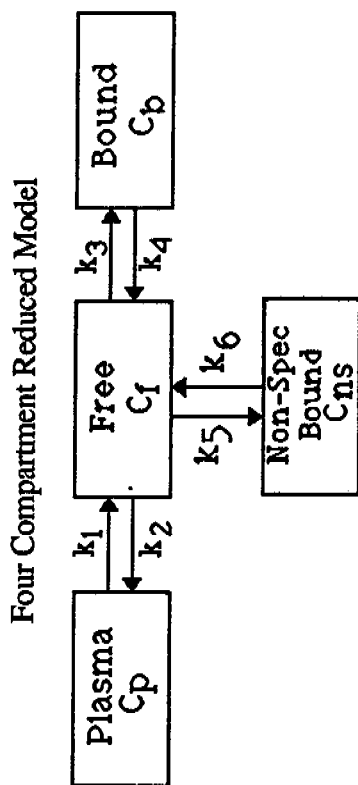


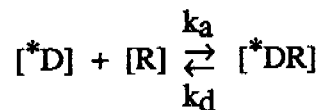
Figure 2. Four or three compartment model utilized for the analysis of PET receptor binding data *in vivo*.  $C_p$  is the plasma concentration of labelled ligand,  $C_f$  is the tissue concentration of free, labelled ligand,  $C_{ns}$  is the tissue concentration of non-specifically bound, labelled ligand,  $C_b$  is the tissue concentration of specifically bound, labelled ligand, and  $k_1$  through  $k_6$  are the rate constants describing the transfer between compartments. All rate constants are first order except  $k_3$  which is a pseudo-first order constant for tracer doses of ligand.

1. The delivery of ligand to the tissues is independent of blood flow; therefore, the blood flow term can be eliminated. This is generally the case when  $k_1$  is relatively small.
2. The transport across the capillary walls (e.g., blood-brain barrier) is a first-order process (i.e., a diffusional process or a high-capacity carrier system).
3. The free ligand in tissue is in equilibrium with the non-specifically bound ligand in tissue.

When the non-specific binding is readily reversible (i.e.,  $k_5$  and  $k_6 \gg k_3$ ), the free and non-specifically bound tracer can be assumed to exist in a common compartment,  $C_f$  (i.e., the free ligand in tissue is kinetically indistinguishable from the non-specifically bound ligand in tissue), resulting in the three compartment model pictured in Figure 2.

Although the model is conceptualized in a compartmental format, it is not a true compartmental model since  $k_3$  is not a true first-order parameter<sup>86</sup>. The  $k_3$  parameter represents the rate constant for a capacity-limited process. Therefore,  $k_3$  is a pseudo-first order parameter when trace amounts (i.e., very small amounts relative to the number of available receptors) of ligand are present. Although the compartmental format is useful from a conceptual viewpoint, the receptor-binding model is more accurately described by the series of differential equations that describe the transfer and binding processes. See Appendix 3 for a more complete explanation.

The binding of labeled tracers to physiological receptors can be described by the law of mass action<sup>87-88</sup>:



where

$[*D]$  = concentration of free labeled ligand, also known as F  
(free)

$[R]$  = concentration of unoccupied receptors

$[*DR]$  = concentration of labeled ligand-receptor complex, also  
known as B (bound)

$k_a$  = association rate constant

$k_d$  = dissociation rate constant

which describes a bimolecular association followed by a unimolecular dissociation.

The affinity of the ligand for the receptor is described by the  $K_D$ , the equilibrium dissociation constant:

$$K_D = \frac{[*D][R]}{[*DR]} = \frac{k_d}{k_a}$$

which can be calculated from the equilibrium concentrations of the interacting species or from the ratio of the dissociation and association rate constants,  $k_d$  and  $k_a$ , respectively.

PET receptor-binding data have traditionally been analyzed by one of two approaches<sup>71-74,79,81,83,89</sup>: 1) Dynamic approach (See Appendix 3.) and 2)

Equilibrium approach.

In the dynamic approach, the compartmental model with the corresponding differential equations is utilized. In the equilibrium approach, the parameters of interest in ligand-receptor interactions,  $K_D$  and  $B_{max}$ , are determined from the concentrations of the specifically-bound (B) and free (F) ligand at equilibrium.

When the system attains equilibrium, the rate of association is equal to the rate of dissociation. The above expression can be rearranged and re-parameterized to include the total receptor concentration, referred to as  $[R]_{\text{total}}$  or  $B_{\text{max}}$ :

$$[*DR] = \frac{[*D] ([R]_{\text{total}} - [*DR])}{K_D + [*D]}$$

If "tracer" quantities of ligand are employed, the number of bound receptors is mathematically insignificant to the total number of receptors present ( $[*DR] \ll [R]_{\text{total}}$ ). In practice, investigators frequently consider values of  $[*DR]$  less than 10% of  $[R]_{\text{total}}$  to fulfill this assumption<sup>88</sup>. Under this condition, the expression can be simplified to:

$$[*DR] = \frac{[*D] [R]_{\text{total}}}{K_D + [*D]}$$

or

$$B = \frac{F B_{\text{max}}}{K_D + F}$$

and in the linear form:

$$\frac{B}{F} = \frac{B_{\text{max}}}{K_D} - \frac{B}{K_D}$$

where  $B = [*DR]$  = concentration of labeled ligand-receptor complex, and  $F = [*D]$  = concentration of free labeled ligand. The data are generally analyzed by applying a Scatchard analysis (i.e., a plot of  $\frac{B}{F}$  versus  $B$  which yields a slope =  $-\frac{1}{K_D}$  and y-intercept =  $\frac{B_{\text{max}}}{K_D}$ ). A minimum of two data points determined at two different tracer concentrations (i.e., two separate studies) is required for the determination of the parameters of interest via this linearized method. Alternatively, the use of a nonlinear method would require additional data points.

Receptor occupancy by a therapeutic agent can be calculated by determining the change in the bound versus free ratio of a reference agent<sup>78,90</sup>. The theory underlying this method is that the reduction in the number of available receptors is proportional to the reduction in the ratio  $\frac{B^*}{F^*}$ . This relationship can be used to calculate the percent receptor occupancy (R):

$$R = \left[ \frac{B^*}{F^* \text{ ref}} - \frac{B^*}{F^* \text{ drug}} \right] \times \frac{100}{\frac{B^*}{F^* \text{ ref}}}$$

where  $\frac{B^*}{F^* \text{ ref}}$  = reference ratio with no drug present and  $\frac{B^*}{F^* \text{ drug}}$  = observed ratio after drug treatment. For the dopaminergic system, the receptor type, agent and reference values used are:

Dopamine D <sub>2</sub> receptor	[ <sup>11</sup> C]raclopride	3.04
Dopamine D <sub>1</sub> receptor	[ <sup>11</sup> C]SCH23390	1.96

Results of the application of this methodology are presented in a later section (Receptor Binding and Occupancy: Dopamine-D<sub>2</sub> Receptors).

**Non-compartmental Analysis: Mean Transit Time**

The clearance rate constant, k, can be calculated using statistical moment theory via the determination of mean transit time<sup>45,91</sup>. Since the drug or tracer concentration in plasma or a particular tissue can be regarded as a statistical distribution curve, the first three moments (zero, first and second) are the area-under-the-curve (AUC), mean residence time (MRT), and the variance of the mean residence time (VRT), respectively. These moments are defined mathematically by the following equations<sup>91</sup>:

$$AUC = \int_0^{\infty} Cdt$$

$$\text{MRT} = \frac{\int_0^{\infty} tCdt}{\int_0^{\infty} Cdt} = \frac{\text{AUMC}}{\text{AUC}}$$

$$\text{VRT} = \frac{\int_0^{\infty} t^2 Cdt}{\int_0^{\infty} Cdt} = \frac{\int_0^{\infty} (t - \text{MRT})^2}{\text{AUC}}$$

The MRT is analogous to half-life in that it represents the time for 63.2% of the drug or tracer to be removed from the compartment. For a one compartment model with IV bolus administration, the relationship between MRT and  $k$ , the first-order elimination rate constant is:

$$\text{MRT} = \frac{1}{k}$$

For multicompartmental systems, measured MRT multiplied by 0.693 is equivalent to the effective half-life of the drug. The calculation of a rate constant via mean residence time or mean transit time has the advantages of numerical simplicity (i.e., no nonlinear curve-fitting required) and relative robustness when the data are noisy.

In the application of statistical moment theory to [ $^{11}\text{C}$ ]acetate, Choi<sup>45</sup> refers to the first moment as the mean transit time or  $\bar{t}_1$ . Because of the additive property of the first moment, the true mean transit time can be determined even when the input to the tissue of interest is delayed.

$$\bar{t} = \frac{\int_0^{\infty} tC_i(t)dt}{\int_0^{\infty} C_i(t)dt} - \frac{\int_0^{\infty} tC_b(t)dt}{\int_0^{\infty} C_b(t)dt} = \bar{t}_1 - \bar{t}_d$$

where  $C_i(t)$  = the tissue concentration over time and  $C_b(t)$  = the arterial blood concentration over time, and  $\bar{t}_d$  is the delay time.

$$\bar{t} = \bar{t}_1 - \bar{t}_d = \frac{1}{k} = \text{MRT}$$

If truncated data are used, corrections to the above relationships must be employed.

Mean transit time or mean residence time values are also used in radiation dosimetry calculations<sup>92</sup>.

### Non-compartmental Analysis: Standardized Uptake Values (SUV)

Standardized uptake value (SUV), also referred to as DUR (dose uptake ratio, differential uptake ratio) or DAR (dose absorption ratio, differential absorption ratio), is a measure of the amount of tracer taken up into a particular tissue normalized by the dosage of tracer administered and the weight of the patient.

The usual equation for SUV<sup>93</sup> is:

$$\text{SUV} = \frac{\text{radioactivity concentration [Bq cm}^{-3}\text{]}}{\text{injected dose [Bq]} / \text{weight of the patient [g]}}$$

Careful consideration must be paid to the units in this equation. If the ROI (region-of-interest) or pixel values are not displayed in concentration units that inherently factor in time and the conversion between scanner measurements and activity, the duration of imaging and pre-determined calibration factors must be factored into the equation. For example, a reconstruction algorithm that displays images in PET counts/pixel would use the following equation for calculation of an SUV value:

$$\text{SUV} = \frac{\text{radioactivity concentration [PET counts/pixel]} \times \text{Calibration factor } (\mu\text{Ci/cc/ct/pixel/s})}{\frac{\text{Image duration [sec]} \times \text{injected dose } [\mu\text{Ci}]}{\text{weight of the patient [g]}}}$$

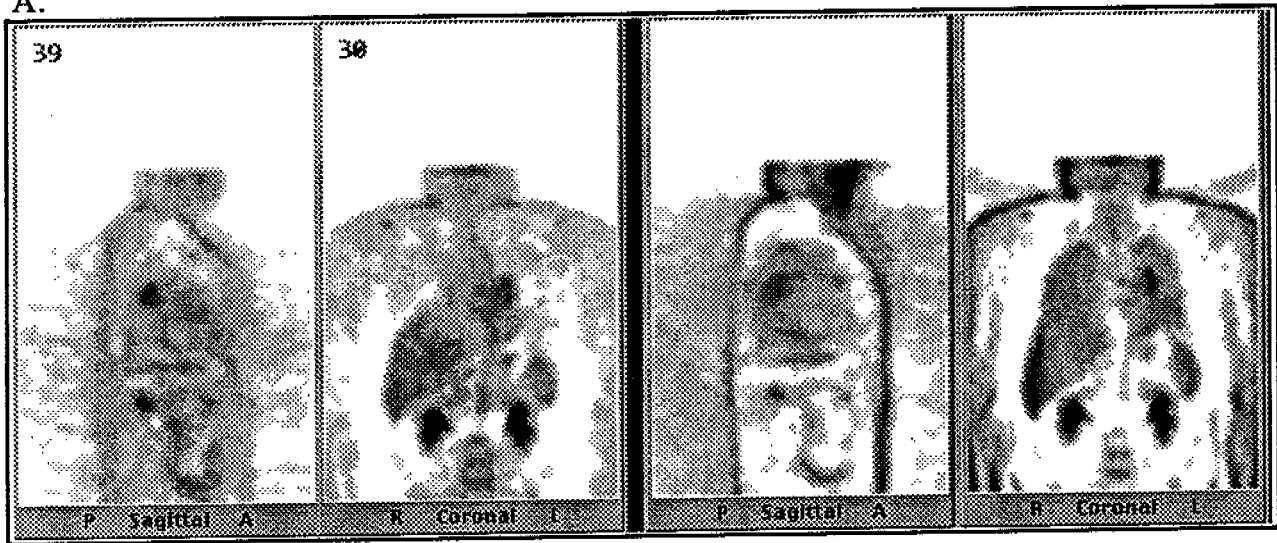
The assumption that  $1 \text{ cm}^3 = 1 \text{ g}$  is generally made. Alternatives to the above equation have employed the use of lean body mass<sup>94</sup> or body surface area<sup>95-96</sup> in lieu of actual body weight.

Although SUVs are semi-quantitative measures that can theoretically be utilized for any tracer that undergoes "trapping" within the tissues, the most frequent usage of SUVs is in the evaluation of clinical whole-body FDG images. The SUV can be a useful piece of information, however, a number of factors influence the magnitude of the SUV<sup>97</sup>:

**Attenuation correction.** SUVs are only valid on attenuation-corrected images. Non-attenuation corrected images will inherently have a concentration gradient dependent solely on the distance of the pixel from the surface of the body. For example, the skin appears very "hot" on non-attenuation-corrected images, essentially outlining the body. (See Figure 3.) An SUV calculated from a relatively superficial lesion will have a significantly larger value than an SUV calculated from a deeper structure, even if the uptakes of the two lesions are identical. Therefore, without attenuation correction, SUVs should not be calculated.

**Patient size.** Calculation of SUVs using total body weight assumes that all individuals have the same "normal" distribution of tracer. However, fat tissues have lower uptakes of FDG and other tracers, resulting in distributions of SUVs correlated not just with tracer uptake, but with subject body weight also. The use of lean body mass offers a slightly better approach. Alternative normalization schemes that employ body surface area appear to be the least dependent on patient characteristics<sup>96</sup> and are the most reliable indicators of actual tracer uptake.

A.



B.

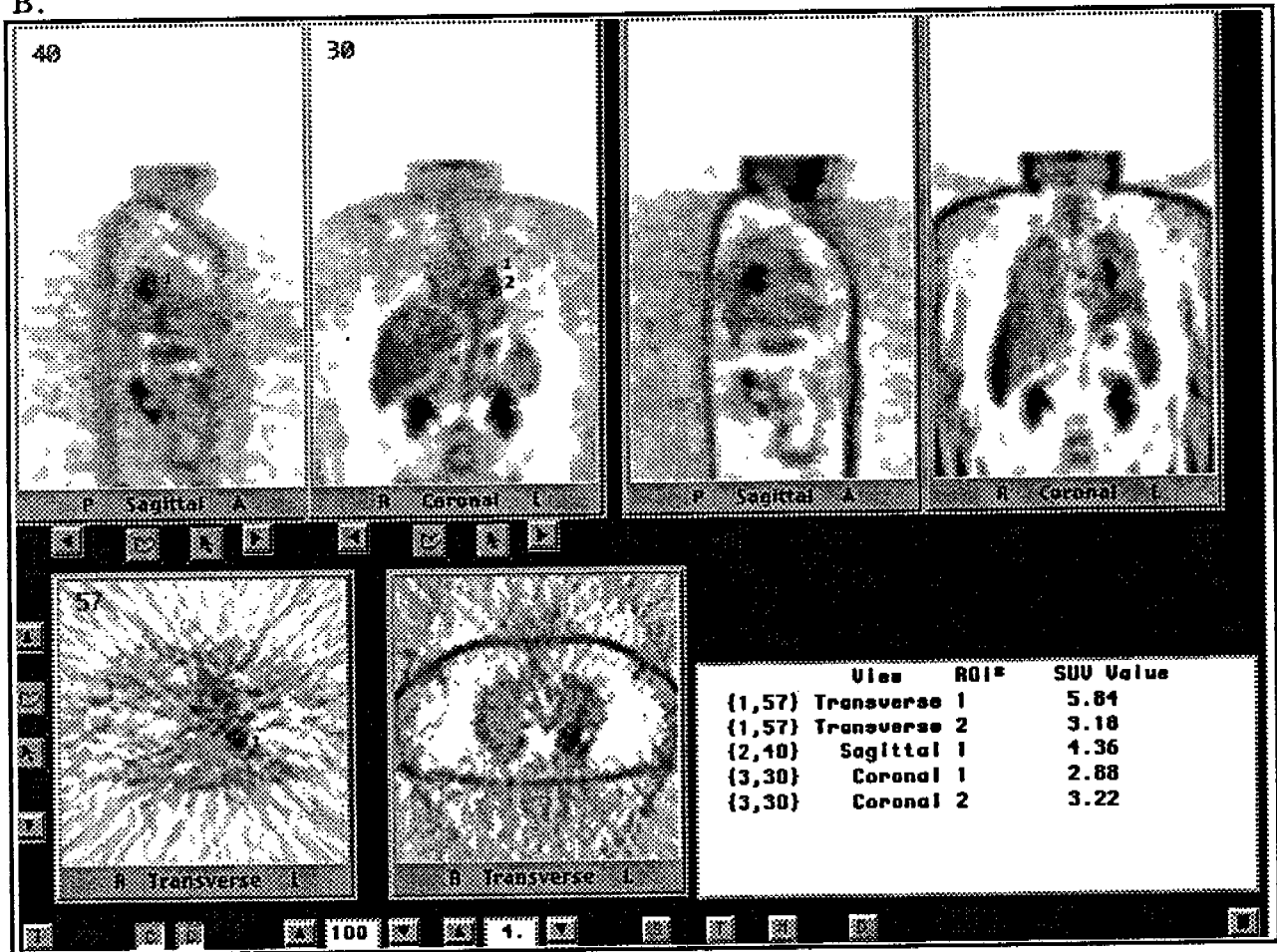


Figure 3. Example of a clinical FDG study of a patient with a solitary pulmonary nodule. "A" illustrates the differences between attenuation-corrected (left panels) and non-attenuation-corrected (right panels) for sagittal and coronal whole-body images. "B" illustrates the clinical display screen used. All three orthogonal views are routinely displayed with and without attenuation correction.

However, the majority of clinical research has been reported using the SUVs calculated from body weight.

**Imaging time.** For tracers that are completely extracted in a first pass and undergo no redistribution, only tracer decay will need to be factored into an SUV calculation. However, when an on-going metabolic process is being imaged, the uptake, and therefore, the SUV is time dependent. Within the acquisition time of a whole-body FDG scan, tracer concentration will increase due to continued uptake and phosphorylation and decrease due to decay and in some tissues, dephosphorylation. Therefore, within a particular facility, standard imaging times with decay correction should be employed to optimize the comparability of SUVs. Generally, imaging begins no earlier than 30 - 45 minutes post-injection (earlier for brain and later for body imaging) and is limited to 90 - 120 minutes for both emission and transmission imaging<sup>52</sup>.

**Plasma glucose levels.** FDG is an analogue of glucose which utilizes the same metabolic pathways as glucose. Glucose competes with FDG resulting in lower SUVs with increased plasma glucose levels<sup>93,98</sup>. Therefore, whole-body oncology imaging is generally performed in the fasting state (minimum of 4 hour fast) to minimize this competition. Glucose levels should be measured in all patients prior to FDG injection to ensure that levels are within the normal range for fasting (i.e., 60 - 120 mg/dl). Plasma glucose levels above 130 mg/dl have resulted in reduced diagnostic accuracy<sup>98</sup>. Diabetic patients must be normoglycemic prior to the PET study. If the patient has a plasma glucose above the desired level, insulin should not be administered to bring the glucose level down because this will force the FDG into insulin-dependent tissues such as the heart, liver and skeletal muscle.

Instead, the advisable course is to wait to see if the plasma glucose level drops naturally or to re-schedule the procedure for another day. These recommendations apply only to whole-body oncologic imaging where SUVs are important semi-quantitative, adjunctive information to the qualitative image appearance in reaching a diagnosis.

Differences exist in tissues that normally are highly metabolically active such as brain and heart. Ishizu, et al.<sup>99</sup>, found improved tumor-to-cerebral cortex ratios and better tumor visualization with glucose-loading. Cardiac imaging requires insulin to facilitate FDG uptake, therefore, the patient is administered glucose and/or insulin prior to tracer administration. At the University of Iowa, 91 whole-body FDG studies performed in the fasting state were examined for cardiac uptake. Fifty-two (57%) had visualized uptake in the left ventricle (LV). The average whole blood glucose level at the time of injection was  $74.1 \pm 23.7$ ,  $73.2 \pm 26.7$ , and  $75.2 \pm 22.2$  mg/dl for all studies, and the subsets of studies for which the LV was and was not visualized, respectively. Five of the patients had studies performed on more than one occasion. In two of these patients, the LV was visualized on one but not the other study. In the two patients in which the LV was visualized in both studies, the mean difference in SUV was 5.4, with essentially no difference in fasting glucose levels. One subject did not visualize the LV on either study. Cardiac visualization on whole-body FDG imaging exhibits a large degree of unexplained intra- and intersubject variability<sup>100</sup>.

**Partial volume, ROI and recovery coefficient effects.** The recovery coefficient is the fraction of true activity measured or “recovered” in the reconstructed image of an object. The recovery coefficient (RC) is a function of the

size of the object, with objects less than twice the resolution of the imaging system exhibiting RC values significantly less than 1. Partial volume effects refers to the fact that tomographic images do not segment along tissue-specific lines, but rather a given pixel is potentially a mixture of tissues. Again, partial volume effects are size-dependent. Larger objects are more likely to have a greater number of pixels that consist of only the tissue of interest than are smaller objects. Since SUVs are generally calculated for ROIs circumscribing a particular tissue or lesion, the size and shape of the ROI will determine the magnitude of the SUV.

Since all three of these factors influence the SUV, carefully drawn ROIs following the margins of a lesion that is relatively homogeneous and larger than twice the resolution of the scanner will produce the most accurate and reliable measurements. Small lesions may appear "colder" (or "hotter" if it is a "cold" lesion in a "hot" field) and have lower SUVs (or higher) than would be calculated for a larger lesion with the same tracer concentration because of the recovery coefficient, partial volume effects, and the mechanical difficulty in creating an appropriate ROI. The use of maximum, rather than mean, pixel values for lesion-based SUVs minimizes the later problem but does not eliminate the first two.

Figure 3 illustrates the use of SUV in an FDG study of a patient with a solitary pulmonary nodule. Figure 3a is a side-by-side comparison of attenuation-corrected and non-attenuation-corrected sagittal and coronal images. Note the differences in the relative activity in the skin, neck area, mediastinum and lateral aspects of the liver between the two sets of images. Figure 3b represents the clinical display format utilized at the University of Iowa. ROIs are drawn on various image sets and the corresponding maximum SUV is displayed in the lower

right-hand box. The software limits the user to SUV calculations on attenuation-corrected images only. Note that on the non-attenuation-corrected images the lesion appears to be a "solitary" nodule, whereas, with attenuation-correction, the coronal display shows two separate lesions.

SUVs represent useful adjunctive information in the clinical decision-making process. However, with all of the problems (detailed above) associated with the calculation of FDG SUVs, their use as hard and fast criteria for the differentiation of benign from malignant tissue is unwarranted.

#### **Non-compartmental Analysis: Multiple-Time/Graphical Approach (The Patlak Method)**

The use of compartmental approaches for the modeling of PET radiopharmaceutical disposition can potentially become conceptually unwieldy and numerically cumbersome. Since the process of interest frequently is an end-stage event resulting in an irreversible or nearly irreversible trapping of the tracer within the system (compartment), a non-compartmental approach, known as the multiple-time/graphical analysis or the Patlak Method, has been developed for the evaluation of transfer constants through a graphical analysis of multiple time data points<sup>101-102</sup>.

Conceptually, this approach has three components:

1. Source (generally the plasma) – which communicates with the other components of the model.
2. Reversible compartments – which consists of n compartments which all freely communicate with one another (and therefore can be considered to be a single compartment), and

communicates bidirectionally with the plasma, and, potentially, unidirectionally with the irreversible component.

3. Irreversible compartments – which consists of one or more compartments which communicate unidirectionally (i.e., traps) with the plasma and, potentially, the reversible component.

Application of this method requires the following assumptions<sup>101</sup>:

1. The plasma represents the sole source of the tracer, the concentration of which may vary with time.
2. The exchange between the reversible component and the plasma is relatively rapid and governed by first-order kinetics. All tracer which enters this region can exit only by returning to the plasma or by entering the irreversible region.
3. All tracer entering the irreversible component becomes functionally trapped within this region. If the tracer undergoes metabolism within the system, it occurs only within the irreversible component and produces a metabolite that is trapped at this stage.
4. The tracer, at the concentration used, does not perturb or alter the system being investigated.
5. At time = 0, the concentration of the tracer in both the reversible and irreversible components of the system = 0.

The overall uptake rate constant or influx constant,  $K$ , can be defined by the following relationship<sup>102</sup>:

$$K = \frac{A_m(\infty)}{\int_0^{\infty} C_p(t) dt}$$

where  $A_m(\infty)$  = amount of tracer trapped in the system at infinite time, and  $C_p(t)$  = plasma concentration at time = t. At  $t^*$  the amount of tracer in the reversible compartments will be effectively at steady-state with the plasma. This time is defined by the nature of the reversible compartments. For time  $t > t^*$ , the following equation is valid:

$$A_m(t > t^*) = K \int_0^t C_p(\tau) d\tau + (V_o + V_p)C_p$$

where  $V_o = fV_e$  = relative fraction in the reversible compartments (a constant) x steady-state volume of the reversible compartments. Rearrangement of this equation yields:

$$\frac{A_m(t)}{C_p(t)} = K \frac{\int_0^t C_p(\tau) d\tau}{C_p(t)} + (fV_e + V_p)$$

A plot of  $\frac{A_m}{C_p}$  versus  $\frac{\int_0^t C_p d\tau}{C_p}$  will become a straight line at  $t = t^*$  with a slope = K and a ordinate intercept =  $(V_o + V_p)$ .  $(V_o + V_p)$  is a positive number which defines the plasma space plus the lower limit of the volume of the rapidly reversible space. An example of a Patlak plot utilized to calculate the global glucose metabolic rate from dynamic  $[^{18}\text{F}]$ fluorodeoxyglucose (FDG) data is presented in Figure 4.

The Patlak Method has been utilized to analyze myocardial glucose utilization with  $\text{FDG}^{103}$ , the binding of N- $[^{11}\text{C}]$ methylspiperone to dopamine- $\text{D}_2$

### Patlak Plot

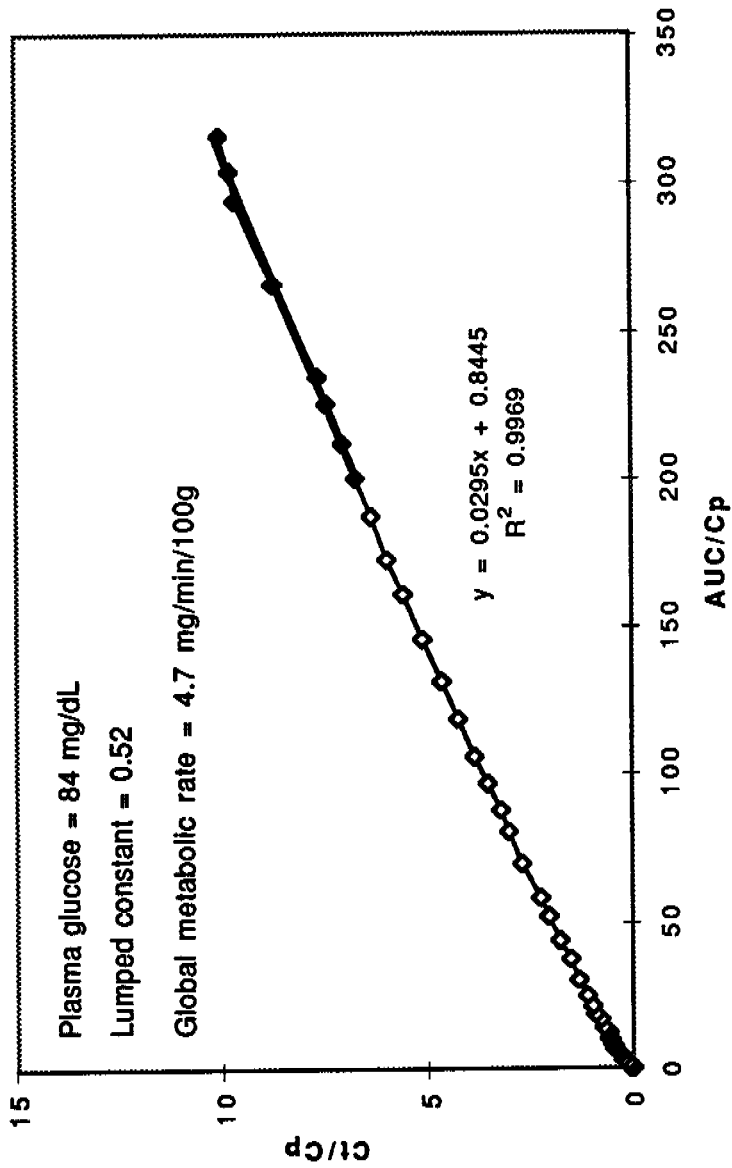


Figure 4. Example of Patlak plot used for the calculation of whole-brain glucose metabolic rate in a research patient.  $C_t$  = tissue concentration at time =  $t$ ,  $C_p$  = plasma concentration at time =  $t$ ,  $AUC$  = area under the plasma concentration versus time curve up to time =  $t$ . The bold line and corresponding regression equation represent the fit of the data at steady-state through end of data acquisition (time = 45 - 60 minutes).

receptors<sup>71-72</sup>, the turnover of brain monoamine oxidase with L-[<sup>11</sup>C]deprenyl<sup>104</sup>, and amino acid transport in the human brain<sup>105</sup> and tumor with L-[<sup>11</sup>C]methionine<sup>106</sup>.

### The Use of PET in Pharmacokinetics

The importance of pharmacokinetic modeling to the analysis of PET-acquired data was detailed above and related to specific models/applications. The use of PET imaging as a pharmacokinetic tool involves the labeling of the drug of interest and the subsequent imaging and analysis of the time-course of the agent's disposition. Because of chemical, physical, and biological constraints inherent in this approach, as described below, applications have been relatively limited. This approach has been employed primarily for receptor-binding ligands, especially those that bind to receptors in the central nervous system, and cancer chemotherapeutic agents.

The use of PET imaging as a pharmacodynamic tool involves the imaging and analysis of the degree and time-course of pharmacologically-induced modifications in fundamental biological processes such as blood flow and/or metabolism. This approach is applicable whenever the pharmacological or toxicological effect involves the induction of change in one of these fundamental processes (e.g., investigations into the effect of  $\alpha_2$  receptor agonists on myocardial perfusion utilizing successive <sup>82</sup>Rb dynamic PET studies<sup>107</sup>; effect of adenosine on cerebral blood flow utilizing [<sup>15</sup>O]water<sup>108</sup>; imaging of fenfluramine-induced changes in the serotonergic system with FDG<sup>109</sup> and [<sup>15</sup>O]water<sup>110</sup>. In contrast to

the relatively limited application of PET as a pharmacokinetic tool, the application of PET imaging for the assessment of pharmacodynamics is essentially an area of unlimited potential.

The topic of positron emission tomography studies of pharmacokinetics was reviewed previously by Yamamoto and Diksic<sup>111</sup>. They examined the subject from a pharmaceutical transport perspective. In contrast, this review will present representative examples of the types of pharmacokinetic/dynamic issues that can only be addressed, *in vivo*, by PET imaging.

#### **“Imageable Biodistribution”: General Considerations**

To the pharmacokineticist, the potential of having a labeled compound with imaging capability represents the potential to actually “see” the hypothesized drug distribution. However, to bring this potential to reality, a number of criteria must be met.

1. The chemical synthesis and quality control testing must be completed within 2 to 3 half-lives of the nuclide. For [<sup>11</sup>C] compounds, this time limit is one hour. For [<sup>18</sup>F]-containing compounds, this time limit can be as long as 5.5 hours.
2. The label must remain a part of the active moiety.
3. The pharmacokinetics of interest must be observable within 2 to 3 half-lives.
4. The region-of-interest (i.e., kinetic “compartment”) must be larger than the resolution of the scanner (e.g., 6 mm).

When these criteria can be met, acquisition of information, essentially unobtainable by other means, is possible. Examples of the pharmacokinetics of [ $^{18}\text{F}$ ]fluconazole and [ $^{18}\text{F}$ ]fleroxacin were detailed by Babich and Callahan in Volume V, Lesson 6. Drug delivery, biodistribution and kinetics of nasally-administered triamcinolone acetonide (Nasacort®) and fluticasone propionate (Flonase®) have been studied using the  $^{11}\text{C}$  and  $^{18}\text{F}$ -labeled drugs, respectively<sup>112-113</sup>. In addition, Searle has used whole-body PET images of the distribution of [ $^{18}\text{F}$ ]lomefloxacin in advertising for their product, Maxaquin®.

### **CNS Pharmacokinetics/dynamics**

Medically intractable epilepsy is a significant problem<sup>114</sup>. Both pharmacokinetic as well as pharmacodynamic explanations can be hypothesized as causes of medically intractable conditions. Baron, et al.<sup>115</sup> studied 10 subjects, 8 with intractable partial epilepsy and 2 non-epileptics, with [ $^{11}\text{C}$ ]phenytoin. Large amounts of labeled phenytoin penetrated the brain nearly immediately with the early images resembling cerebral blood flow maps. In the non-affected hemisphere, the gray matter reached equilibrium within 20 minutes, but the white matter continued to have a rising concentration, even after 60 minutes. The brain-blood concentration ratios at 50 minutes were 1.37 and 1.06 for gray and white matter, respectively. These values are similar to concentration ratios observed in tissue samples acquired at surgery. There was no evidence that normal brain regions of treatment-resistant epileptics bind phenytoin less effectively than non-epileptics. Since brain and blood concentrations of [ $^{11}\text{C}$ ]phenytoin were well correlated, blood levels of phenytoin are reliable estimates of the brain concentrations of the drug.

Therefore, in the case of phenytoin, medical resistance to treatment is not considered to be of a pharmacokinetic, but rather is of a pharmacodynamic origin.

The use of PET imaging in epilepsy has recently been reviewed by Henry<sup>116</sup>. Pharmacodynamically, the older anticonvulsant agents are known to decrease global cerebral glucose metabolic rates (gMRGlc) as determined by FDG imaging and cerebral blood flow as determined by [<sup>15</sup>O]water imaging<sup>117</sup>. The degree of reduction in gMRGlc is similar to the side effect profile of the agents with phenobarbital (37%)<sup>118</sup> > valproate (22%)<sup>119</sup> > phenytoin (13%)<sup>120</sup> = carbamazepine (12%)<sup>121-123</sup>. The newer anticonvulsants have different mechanisms of action (e.g., GABAminergic) and side effect profiles than the older agents. The effect of these agents on global cerebral physiology has not been studied.

#### **Route of Administration: I.A. versus I.V.**

A critical objective of any treatment regimen, but especially for those regimens involving highly toxic drugs such as cancer chemotherapeutic agents, is to maximize the desired responses (i.e., therapeutic responses) while minimizing undesirable responses (i.e., side effects and toxicological effects). One of the choices which potentially influences this "therapeutic balancing act" is that of the route of administration.

The "pharmacological advantage" (defined as the ratio of the integrated tumor/brain count ratios) of I.A. (intra-arterial) versus I.V. (intravenous) administration of two cancer chemotherapeutic agents, cisplatin (DDP) and carmustine (BCNU) has been evaluated for central nervous system tumors using the [<sup>13</sup>N] and [<sup>11</sup>C] labeled derivatives, respectively<sup>124-125</sup>. The intracarotid

administration of cisplatin produced 1.1 to 2.5 times greater tumor/brain ratios than did I.V. administration<sup>124</sup>. Super-selective arterial administration (i.e., administration through the artery known to be the major tumor-feeding vessel) of BCNU provided tumor-to-normal brain ratios of 50:1, whereas, I.V. administration provided ratios of only 1.2:1<sup>125</sup>. Furthermore, ratios of tumor [<sup>11</sup>C] radioactivity concentrations between the I.A. and I.V. routes ranged from 2.5 to 99 (n = 10). The two highest ratios were associated with the patients demonstrating the most dramatic responses, and the lowest ratios were associated with individuals experiencing essentially no therapeutic response.

Similar investigations have been undertaken to evaluate the regional administration of 5-fluorouracil (FU) in the treatment of metastatic liver disease<sup>126</sup>.<sup>128</sup> Examination of the short- and long-term uptake of 5-[<sup>18</sup>F]fluorouracil into metastatic lesions after I.V. and I.A. administration demonstrated that enhanced drug exposure through regional administration was only one of the factors involved in determining potential responsiveness to therapy. For FU, preferential perfusion must also be accompanied by high tumor cell transport and metabolism. Therefore, delivery of the therapeutic agent, in this case FU, to the tumor is a necessary but not a sufficient predictor of response<sup>126,129-130</sup>. The sources of error in [<sup>18</sup>F]5FU pharmacokinetic analyses were evaluated by Harte, et al.<sup>131</sup>.

## Receptor Binding and Occupancy

**Dopamine-D<sub>2</sub> Receptors:** Pharmacokinetic/dynamic investigations rely heavily on drug concentration levels measured in accessible body fluids such as serum, plasma, whole blood, saliva, and/or urine. The use of these measures is

predicated on the assumption that the concentrations in these fluids reflect the concentration at the site of action. Whenever the response pattern mirrors the concentration pattern in the measured fluid, this assumption is reinforced. Whenever an inconsistent relationship is exhibited, the assumption is in question and a more direct measure is necessary.

The antipsychotic effect of neuroleptic drugs is believed to be due to the ability of these agents to block central dopamine receptors<sup>132-133</sup>. Unfortunately, plasma levels of neuroleptic agents are known to be imperfect predictors of response<sup>134-136</sup>. Therefore, studies utilizing PET imaging have taken a more direct approach to the examination of the issues surrounding neuroleptic treatment. Specifically, three issues have been examined with respect to dopamine-D<sub>2</sub> receptors and neuroleptic therapy<sup>78,137-138</sup>:

1. What degree of receptor blockade is induced by clinically-administered dosages of various neuroleptic agents?
2. What is the time-course of receptor occupancy and plasma levels upon neuroleptic withdrawal?
3. Do responders and non-responders differ in neuroleptic-induced receptor blockade?

Using [<sup>11</sup>C]raclopride, Farde, et al.<sup>78</sup> studied central dopamine-D<sub>2</sub> receptor occupancy in 14 schizophrenic patients who had received a single antipsychotic drug, at conventional dosages, for at least one month. Receptor occupancy ranged from 65 to 84% for all agents. In comparison, a single patient receiving nortriptyline experienced no receptor occupancy. The authors concluded that, although all 11 neuroleptics were chemically distinct entities, at typical dosage

levels each induced a 65 to 85% occupancy of central dopamine-D<sub>2</sub> receptors, thus supporting the proposed mechanism of antipsychotic drug action. In addition, the single patient in the study experiencing extrapyramidal side effects (i.e, akathisia), had the highest receptor occupancy at 86% on a dosage of haloperidol of 6 mg BID. After reduction of the dosage to 4 mg BID, the side effects disappeared, but the receptor occupancy remained at 84%. The authors hypothesized that the antipsychotic action may require a lower receptor occupancy than for the development of extrapyramidal effects or that the two effects may be mediated by different receptor mechanisms.

Farde<sup>90</sup> extended this work to look at both dopamine-D<sub>1</sub> as well as dopamine-D<sub>2</sub> binding by examining medicated patients with both [<sup>11</sup>C]raclopride and the selective D<sub>1</sub> antagonist, [<sup>11</sup>C]SCH23390. Classical neuroleptic agents in conventional doses had dopamine-D<sub>2</sub> receptor occupancy of 70 - 80% and did not exhibit any dopamine-D<sub>1</sub> occupancy. Patients experiencing extra-pyramidal symptoms (EPS) had higher dopamine-D<sub>2</sub> receptor occupancies than those without side effects leading to the conclusion that EPS are related to dopamine-D<sub>2</sub> occupancy. Atypical neuroleptics (e.g., clozapine) had dopamine-D<sub>2</sub> occupancy of 38 to 63% and dopamine-D<sub>1</sub> occupancy of 36 - 52%.

Smith et al.<sup>138</sup> utilized an indirect approach to examine the relationship between N-[<sup>18</sup>F]methylspiroperidol (<sup>18</sup>F-NMSP) uptake in the striatum and plasma level in normal subjects and schizophrenic patients treated with either haloperidol or chlorpromazine. The authors found a decrease in affinity of the [<sup>18</sup>F]-NMSP for striatal tissues in the drug-treated schizophrenic patients as compared to the unmedicated control subjects with the magnitude of this decrease directly related to

the antipsychotic drug dose (relative to the clinical potencies of the agents) and plasma level. The ratio index, a measure of receptor occupancy, approached that observed in normal subjects upon withdrawal of the antipsychotic agent. A log-linear relationship was observed between the ratio index (y) and haloperidol plasma levels (x):

$$y = 1.974 e^{-0.082x} \quad r^2 = 0.7482.$$

Utilizing a more direct approach, Farde et al.<sup>78</sup> examined the serial receptor occupancy versus serum drug level upon drug withdrawal in three of the patients described above. In patients treated with sulpiride (600 mg BID) and haloperidol (6 mg BID), the receptor occupancy remained essentially unchanged at approximately 65% and 85%, respectively, after 27 and 54 hours of wash-out, even though the serum drug levels had declined to approximately 25% of initial levels. The third patient underwent step-wise dosage reduction from sulpiride 800 mg BID to 0 mg/day. The receptor occupancy exhibited a curvilinear relationship to total daily dose whereas the serum level exhibited a linear relationship. The authors concluded that the hyperbolic nature of the occupancy curve explained why major changes in drug concentration resulted in only minor changes in the receptor occupancy. Furthermore, they stated that PET imaging may be a method by which minimum individual dosages may be defined which provide adequate receptor occupancy for antipsychotic effects but minimize the potential for adverse effects.

Although the above studies support the concept of a receptor occupancy – response relationship, additional factors may be involved in schizophrenic response to antipsychotic therapy. Wolkin, et al.<sup>137</sup> examined the dopamine-D<sub>2</sub> blockade using [<sup>18</sup>F]-NMSP in two biological subgroups of schizophrenics, responders and

non-responders, treated with a maximum of 100 mg/day of haloperidol (minimum plasma level = 10 ng/mL) for four to six weeks. Comparable levels of haloperidol-induced receptor blockade were found between responders and non-responders. The authors concluded, therefore, that non-response to therapy may not necessarily be caused by inadequate levels of drug in the central nervous system. Instead, responders and non-responders may potentially differ in the pathophysiology of the schizophrenic symptoms and not in the pharmacokinetics of antipsychotic drug disposition.

**Mu-opiate receptors:** The mu-opiate receptor system has been investigated with the opiate agonist, [<sup>11</sup>C]carfentanil<sup>139-140</sup>. Just as with the neuroleptic agents, similar questions regarding degree of receptor blockade and the time-course of occupancy versus plasma levels can be examined with PET. Naltrexone, an orally administered opiate receptor antagonist is utilized in the treatment of narcotic dependency states. Based on [<sup>11</sup>C]carfentanil time-activity curves, the mean percentage blockade of the mu-opiate receptors at 48, 72, 120, and 168 hours post-administration of 50 mg naltrexone was 91, 80, 46 and 30%, respectively<sup>141</sup>. Although naltrexone and its major active metabolite, beta-naltrexol, have apparent plasma half-lives of approximately four and twelve hours, respectively, the effective half-life of receptor occupancy was estimated to be 72 to 108 hours. Thus, the half-time for return to baseline opiate receptor occupancy corresponded more closely with the estimated half-life of the tertiary, terminal phase of the plasma-time activity curve (i.e, 96 hours) and the time-course for inhibition

of the physiologic and subjective effects of heroin (i.e., 72 hours)<sup>141-142</sup> than it did with apparent plasma half-lives.

### **Toxicodynamics: Alcohol**

Alcohol is a drug with a significant potential for toxic effects. Volkow, et al.<sup>143-144</sup> have studied the toxicokinetic/dynamic effects of alcohol in normal subjects (i.e., social drinkers) and in alcoholics with PET imaging. The effects of low (0.5 gm/kg) and moderate (1 gm/kg) alcohol dosages on cerebral blood flow in normal subjects were investigated with [<sup>15</sup>O]water<sup>143</sup>. Scans were performed at baseline and at 40 and 60 minutes post-alcohol ingestion. The results of these scans were compared to blood alcohol levels, subjective measures of intoxication, and scores on a fine motor coordination examination. Although there were no changes in heart rate or blood pressure, subjective measures of intoxication (i.e., "relaxing effect", increased talkativeness, euphoria) started at approximately 20 minutes and peaked at 50 minutes post-administration. All of the subjects experienced impairments in fine motor coordination at the moderate dosage level. After alcohol consumption, a significant relative reduction in blood flow to the cerebellum occurred with a relative increase in blood flow to the prefrontal and the right temporal cortices. The largest effects were recorded at the 60 minute scan when the blood alcohol levels were the highest (i.e., low:  $\bar{X} = 0.044$  mg%, moderate:  $\bar{X} = 0.087$  mg%). The decreases in blood flow to the cerebellum were consistent with the observed disturbances in fine motor coordination. The increased blood flow to the prefrontal and temporal cortices was believed to be related to the observed general mood activation. The authors concluded that the sensitivity of the cerebellar blood flow to the effects of

alcohol could possibly explain the high incidence of ataxia during alcohol intoxication. Furthermore, the cerebral vasoactive response to alcohol could pose a possible explanation for the higher incidence of stroke in "binge" drinkers.

The effect of moderate dosages (1 gm/kg) of alcohol on regional brain glucose transport and metabolism was studied in normal subjects and in alcoholics using FDG<sup>144</sup>. Although there were no significant effects on pCO<sub>2</sub>, pO<sub>2</sub>, or plasma glucose concentrations, the alcohol administration resulted in a significant reduction in brain regional metabolism in cortical areas and cerebellum with relative sparing of the basal ganglia and corpus callosum. The pattern of decreased metabolism reflected the known distribution of benzodiazepine receptors. Examination of the kinetic parameters revealed that the decreased metabolism stemmed from an alteration in k<sub>3</sub> (phosphorylation rate) and not from alterations in either k<sub>1</sub> or k<sub>2</sub> (transport into and out of the brain, respectively). The alcoholic patients experienced a greater decrease in the brain glucose metabolic rate than that experienced by the normal subjects. The authors hypothesized that this finding may be the result of an increased sensitivity of the benzodiazepine/GABA receptor complex in chronic alcoholics.

### **Influence of Enantiomeric Forms**

Drugs that possess an asymmetric carbon atom exist in enantiomeric forms. If the asymmetric carbon is located in a critical area of the molecule (i.e., functional site), the enantiomeric form will influence the corresponding process (e.g., transport, metabolism, receptor binding)<sup>145</sup>. All processes that depend solely on the chemical nature of the molecule (e.g., passive diffusion) are believed to remain

unchanged. Natural products generally exist in the active enantiomeric form only. Synthetic products, on the other hand, generally exist as racemic mixtures, unless specifically purified.

The enantiomeric form of radiopharmaceuticals is important in PET imaging. Inactive enantiomers have played a role in the characterization of non-specific binding in PET receptor-binding studies<sup>77,80</sup>. Their use is predicated on the assumption that all dispositional factors are identical between the enantiomeric forms, with the exception of the specific binding component. In some cases, however, various dispositional processes may be influenced by enantiomeric form. The examples of PET imaging in the study of the disposition of nicotine and cocaine, both natural products and potent central nervous system stimulants, are presented below.

**Nicotine.** The unnatural (+)-(R-) and the natural (-)-(L-) forms of nicotine, labeled with [<sup>11</sup>C], have been utilized to visualize nicotinic receptors in the brain<sup>146-148</sup>. After I.V. administration to humans, the [<sup>11</sup>C] activity peaked in the arterial plasma at 2 minutes and in the brain at 4 - 6 minutes. Plasma levels did not differ between the (+) and (-) forms within individuals, but the steady-state plasma levels did differ between smokers and non-smokers (i.e., slightly higher for smokers). By the end of the imaging period (i.e., 54 minutes), 25% of the (+) form had been metabolized to [<sup>11</sup>C]cotinine, whereas only 15% of the (-) form appeared as the metabolite. Recent studies indicate that this metabolite does not cross the blood-brain barrier<sup>148</sup>. In the brain, the regional distributions of activity resulting from the administration of the (+) and (-) enantiomers were similar, with highest accumulations recorded in the cortical and subcortical regions, and the

lowest in the pons, cerebellum, occipital cortex and white matter of centrum semiovale. Distributional differences were observed between smokers and nonsmokers. The (+) form exhibited a lower peak and a slower decline in activity during the time-course of the study than did the (-) form. The authors hypothesized that these differences were due to different binding profiles of the enantiomers to the nicotinic receptors, and not a complete lack of affinity to the receptor by the unnatural enantiomer.

**Cocaine:** [ $^{11}\text{C}$ ]Cocaine has been utilized to map the cocaine binding sites in the human brain<sup>149</sup>. After I.V. administration, [ $^{11}\text{C}$ ] activity peaked in the brain, specifically the corpus striatum, between 4 - 10 minutes and then declined with a  $t_{1/2}$  of 25 minutes. This pattern paralleled the time-course of cocaine-induced euphoria. In an effort to characterize the non-specific binding, the inactive (+) enantiomer was labeled with [ $^{11}\text{C}$ ], but when administered, resulted in no visible brain uptake<sup>150</sup>. Since the transport of cocaine into the brain is not believed to be stereoselective, alternative explanations were sought. It was found that by 30 seconds post-administration, plasma levels of the (+)cocaine were undetectable. In vitro work found that the (+)cocaine was hydrolyzed primarily to (+)ecgonine methyl ester by butyrylcholinesterase. This enzyme metabolizes the (+) form 2,000 times faster than the (-) form of cocaine. Therefore, the difference in metabolism appears to be a major factor for the distribution differences observed between the enantiomeric forms of cocaine.

## Conclusion

It has been the purpose of this review to acquaint the reader with the uniquely productive relationship between pharmacokinetics and PET imaging. The former provides the necessary tools for image quantitation in the latter, and the latter provides non-invasive, *in vivo* distributional information necessary to address some of the difficult questions confronting investigators in the former. PET imaging has developed into both a tool for and an application of clinical pharmacokinetics/dynamics in the 1990s and beyond.